Nanoscale

RSC Publishing

PAPER

View Article Online
View Journal | View Issue

Cite this: *Nanoscale*, 2013, **5**, 12310

In situ forming, characterization, and transduction of nanowire memristors†

Zheng Fan,[a] Xudong Fan,[b] Alex Li[c] and Lixin Dong*[a]

We report the nanorobotic *in situ* formation and characterization of memristors based on individual copper oxide nanowires (CuO NWs) and their potential applications as nanosensors with memory function (memristic sensors or "memsensors"). A series of *in situ* techniques for the experimental investigations of memristors are developed including nanorobotic manipulation, electro-beam-based forming, and electron energy loss spectroscopy (EELS) enabled correlation of transport properties and dopant distribution. All experimental investigations are performed inside a transmission electron microscope (TEM). The initial CuO NW memristors are formed by localized electron-beam irradiation to generate oxygen vacancies as dopants. Current–voltage properties show distinctive hysteresis characteristics of memristors. The mechanism of such memristic behavior is explained with an oxygen vacancy migration model. The presence and migration of the oxygen vacancies is identified with EELS. Investigations also reveal that the memristic behavior can be influenced by the deformation of the nanowire, showing that the nanowire memristor can serve as a deformation/force memorable sensor. The CuO NW-based memristors will enrich the binary transition oxide family but hold a simpler and more compact design than the conventional thin-film version. With these advantages, the CuO NW-based memristors will not only facilitate their applications in nanoelectronics but play a unique role in micro-/nano-electromechanical systems (MEMS/NEMS) as well.

Received 2nd July 2013
Accepted 24th September 2013

DOI: 10.1039/c3nr03383j

www.rsc.org/nanoscale

Introduction

The first experimental demonstration of a memristor (short for "memory resistor") in 2008 has stimulated quickly expanding interest in nanoelectronics due to its unique circuit properties such as current–voltage hysteresis and time-dependent resistance.[1] Metal oxides, such as TiO_2, Nb_2O_5, NiO and ZnO are the most common raw materials for the fabrication of memristive devices due to their resistive transition behaviors.[2,3] The conventional setup of these materials to be used as memristors uses a thin-film design. These thin-film structured memristors have great advantages such as low-energy electroforming and high switching speed.[2,4] Therefore, they are the natural choice for the next generation non-volatile random-access memory (NVRAM). However, in the thin-film design, the conductive filaments may not be generated in a specific area and the filament length may also not be controlled, which impeded the investigation of the carrier's migrating ability in a memristor device. In our research, we realized memristive switching in a 1D nanostructure and proposed a nanowire-based memristor to study the carrier's migration ability. On the other hand, the interests in nanowire memristors are stimulated by their simpler and more compact design, which will also lead to a higher integration density.[5–7]

As a new fundamental element for electronics, a memristor may also open new possibilities in the development of nanosensors, providing an additional transduction mechanism to piezoresistivity/piezoelectricity, magnetoresistivity, and capacitance.[7] For instance, because a memristor can memorize the voltage applied to it, a memristor-based sensor can record historical information of force/deformation/chemical doping, resulting in a sensor with the ability of memory, or a "memsensor". While a variety of new possibilities for "memsensors" are pending discovery, we tackle the feasibility in this report.

Previous experimental investigations are typically *ex situ*, *i.e.*, the transport properties have been investigated before and after the switching occurred. This is partly due to the setup of the thin-film based memristor where active metal oxide regions are buried under the metal electrode contact, which prevented *in situ* investigation. Furthermore, the thin-film based two-dimensional memristor has limited flexibility to be extended to other forms of devices such as transducers. To understand the memristic switching mechanism, *in situ* investigations on conducting filament growth/dissolution have been reported by

[a]*Department of Electrical and Computer Engineering, Michigan State University, East Lansing, MI 48824, USA. E-mail: ldong@egr.msu.edu; Fax: +1 517 353 1980; +1 517 353 3918*

[b]*Center for Advance Microscopy, Michigan State University, East Lansing, MI 48824, USA*

[c]*Air Force Institute of Technology, Wright-Patterson AFB, OH 45433-7765, USA*

† Electronic supplementary information (ESI) available. See DOI: 10.1039/c3nr03383j

two groups recently.[8,9] Based on these advancements, here we report electron-beam (e-beam) based *in situ* formation of a nanowire memristor and the correlation of its structural changes during the formation and its switching behaviors. All investigations have been performed inside a transmission electron microscope (TEM) using electron beam irradiation, nanomanipulation and electron energy loss spectroscopy (EELS) for its formation, characterization and application. In the following, we will first describe the implementation and characterization of this nanowire-based memristor with nanorobotic manipulation, and then address its mechanism as well as its applications.

Synthesis and forming of the CuO NW-based memristor

1. CuO NW synthesis

The raw materials used for this experiment are as-grown CuO NWs. The synthesis of the nanowires begins with a copper foil.[10] After 2 hours incubation in a box oven at 500 °C (Fig. 1(a)), the non-flaking nanowire arrays were grown on the surface of the copper substrate. The diameters of the nanowires ranged from 30 to 50 nm. The inset I of Fig. 1(a) shows an enlarged scanning electron microscope (SEM) image of a single nanowire. The inset II of Fig. 1(a) also shows that the as-fabricated nanowires are distributed in the substrate at a high density of about 4–6 wires per 100 square nanometers. Furthermore, the high resolution TEM (HRTEM) image (Fig. 1(b)) indicates an inter-planar spacing of 2.53 Å, which demonstrates the excellent crystallinity of the as-synthesized CuO NWs.[11] A single wire was attached on a probe using a nanorobotic manipulator (Fig. 1(c)) installed inside an SEM and then it was fixed in place using focused-ion-beam chemical vapor deposition (FIB-CVD) (Fig. 1(d)). The probe with the nanowire attached acted as a sample holder and was transferred into the TEM for characterization. A scanning tunnelling microscope (STM) holder installed inside the TEM served as a nanomanipulator for the investigation. The nanowire was connected to another probe driven by the nanomanipulator from the other end (Fig. 1(e)), and the electrical properties of this individual nanowire were measured simultaneously. Due to the insulating nature of the CuO NW, the measurement of the as-grown nanowire justified an dielectric behavior, therefore, a forming process is required to actuate the raw nanowires into memristors and enable them with the characteristic memristive switching behaviors.[2,4,5]

2. Forming and characterization

A number of memristor forming processes have been developed in previous investigations.[2,4,6,12] Among them, electroforming[2,6] and physical forming processes[4,12] were most commonly used. However, the electroforming processes are unsuitable for the nanowire-based memristor device since the heat will cause a hard breakdown in the center of the CuO NW due to its cylindrical structure. Likewise, the physical forming is always carried out with several hours of annealing in a furnace, and an inert gas should be injected at the same time, which can hardly be carried out *in situ*. For these reasons, we developed an e-beam-based forming method for the cylinder shaped memristors. By focusing the TEM electron beam on a part of the CuO NW, high energy electrons bombard the nanowire and expel oxygen atoms from the irradiated area in oxide materials.[13] Therefore, the CuO NW will be "de-oxidized". The forming process (Fig. 2(a)) shows that the e-beam is irradiating the nanowire that is fixed between the electrodes using the nanomanipulator. The irradiation current density was adjusted by changing the focus, the magnification, the brightness and the incident area. The empirical procedure of the forming process is: irradiation at a current density of 20 A cm^{-2} on an area of 1.3×10^{-14} cm^2 for 200 s with a spot size of 2 nm. The accelerating voltage of the electron beam was kept at 200 kV in all experiments. The

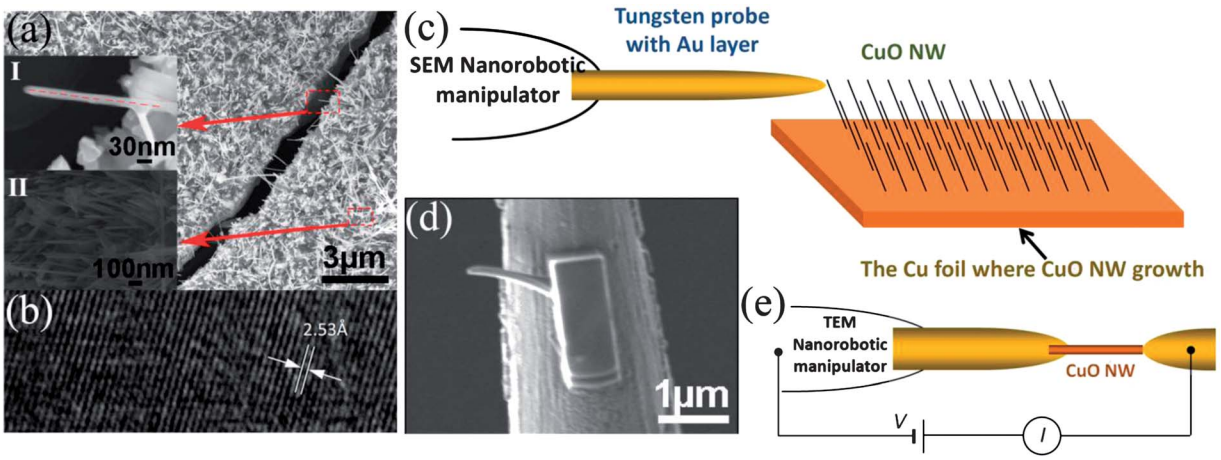

Fig. 1 The fabrication of CuO NWs. (a) The non-flaking nanowire arrays were grown on the surface of the copper substrate after 2 hours incubation in a box oven at 500 °C. Inset I shows the detailed image of a single nanowire. Inset II shows that the as-fabricated nanowires are distributed in the substrate at a high density of about 4–6 wires per 100 square nanometers. (b) HRTEM image indicates an inter-planar spacing of 2.53 Å of the nanowires. (c) A single wire was picked up by a probe using a nanorobotic manipulator installed inside a scanning electron microscope (SEM). (d) The selected nanowire was fixed on the probe by using focused-ion-beam chemical vapor deposition (FIB-CVD). (e) The setup for the electrical characterization of a single CuO NW.

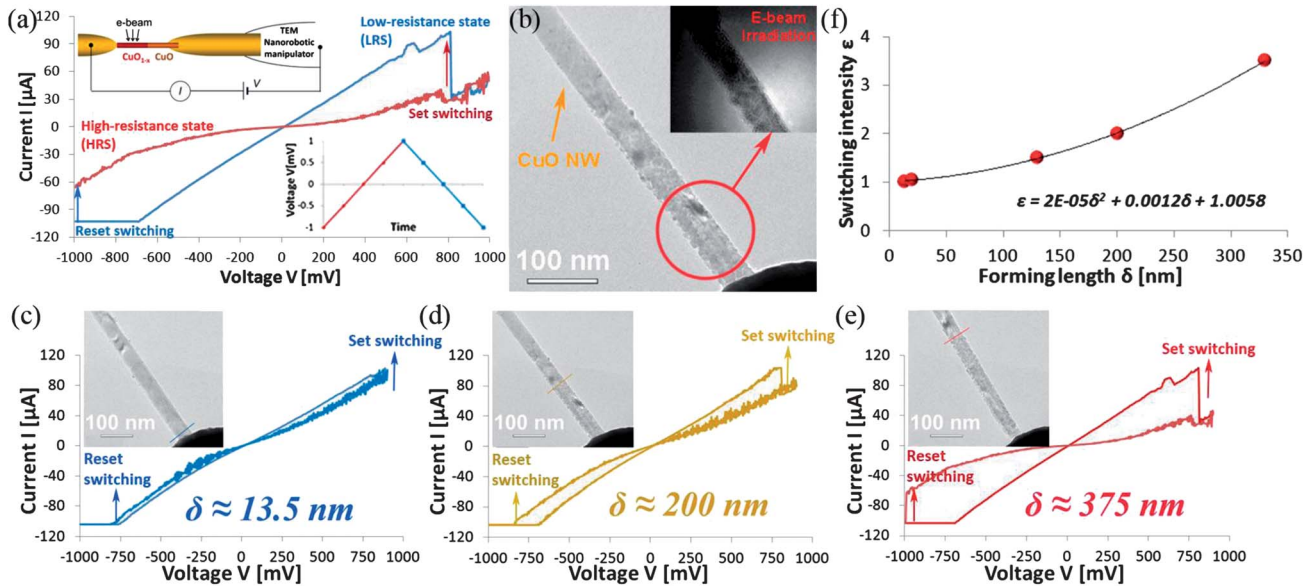

Fig. 2 E-beam-based forming. (a) The schematic of the e-beam-based and the insulator behavior of the original CuO NW was changed to have memristive switching character during forming process. (b) The gradual forming process of the CuO NW, demonstrated by using TEM. (c–e) The switching intensity is increased according to the increase of forming area. (f) The relation between the switching intensity and the forming length is: $= 0.0008^2 + 0.0082 + 1.0036$.

completion of the forming, which actuates the CuO NW to the memristive device, can be identified *in situ* by electrical measurement or microscopy analysis. Since the dynamic resistance is the key characteristic of memristive devices, the hysteresis *I–V* curve (Fig. 2(a)) symbolizes the forming of a memristor device. The HRTEM image (Fig. 2(b)) demonstrates the gradual forming process of the CuO NW with a distinct difference between the metalized segment and the pristine part. The irradiated area tends to become amorphous and can be easily seen from the image.

By analyzing the hysteresis *I–V* curve in Fig. 2(a), it can be noted that there are two distinctive reversible "off" and "on" states in the memristor device. The off state (red curve) corresponds to the high-resistance state (HRS) and the on state (blue curve) corresponds to the low-resistance state (LRS), and their resistances are defined as R_{off} and R_{on}, respectively. When the external bias increased to the 'set' switching threshold voltage ($V_{th} \approx 800$ mV), the device switches from the off state to the on state. As the voltage polarity alternates and the reverse bias reaches the 'reset' switching threshold ($V_{th} \approx -1000$ mV), the device went through a "reset" process change from the on to the off state. In the 'set' process, the cathode was attached to the CuO part and the CuO_{1-x} part was connected to the anode part. In the 'reset' process, the polarity alternates and the cathode in the CuO part switches to the anode and the original anode in the CuO_{1-x} part switches to the cathode. Within the operation voltage, the resistance can be either R_{off} or R_{on}, depending on the memory of the previous applied positive or negative threshold voltage. At high enough voltages that exceed the set or reset thresholds, a memristive device will remain in a fixed state. Furthermore, we can define the magnitude of the switching by ε, the maximum value of R_{off}/R_{on} in a hysteresis dual-curve. For various lengths

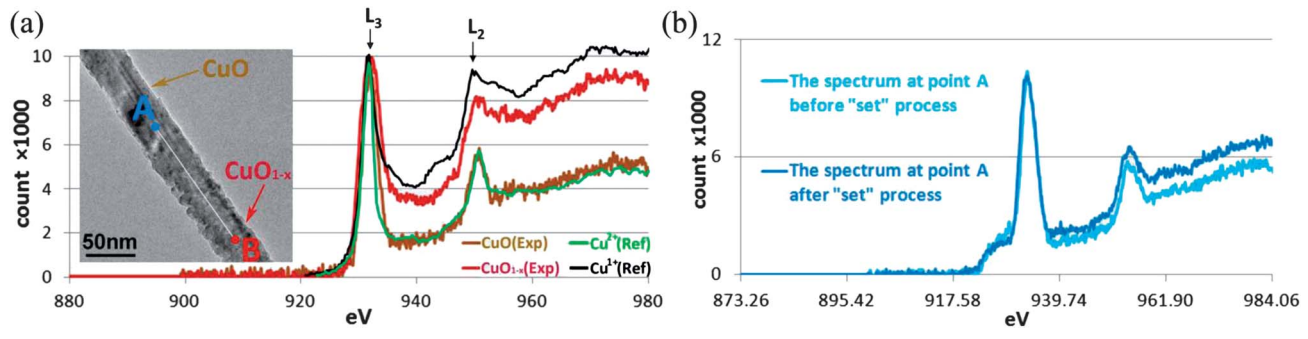

Fig. 3 The characterization of the deoxidized segment. (a) The Cu $L_{2,3}$ edge spectra of the nanowire at point B before and after the electron irradiation, with standard Cu^{2+} and Cu^{1+} spectra superimposed as references. Before the irradiation, the Cu spectrum is coincident with Cu^{2+} very well, proving its 100% CuO composition. The spectrum after the e-beam irradiation shows an intermediate state between Cu^{2+} and the Cu^{1+}. We termed the state as CuO_{1-x} (a mixture of Cu_2O and CuO). (b) The Cu $L_{2,3}$ edge spectra of an unirradiated area at point A before and after the electron "set" process. The higher L_2 peak intensity after the "set" process indicates the presence of more Cu^{1+}, which corresponds to the increase of oxygen vacancies.

δ of the irradiated area, the dynamic *I–V* characteristics are represented as a function of ε (Fig. 2(c)–(e)). It is noted that a small area (*e.g.* ∅ 13.5 nm) of irradiation will be sufficient to induce visible memristive switching behavior. On the other hand, such behaviors may only be visible if the device is at the nanometer scale. A larger irradiation area for forming the memristor will have potentially a larger ε, *i.e.*, a higher switching intensity. Unexpectedly, the threshold voltage V_{th} remains the same. This dynamic process provides an insight into the switching mechanism of CuO NW-based memristive devices.

Memristive switching mechanism

There are several theories explaining the mechanism of memristors.[1,12] It is believed that the CuO NW memristor is functionalized due to the conduction through oxygen vacancy dopants. To verify this, it is critical to justify the oxygen vacancy presence and migration *in situ*. Previous investigations on oxygen vacancies are mainly concentrated on detecting the structural or direct stoichiometry changes.[14,15] Instead of that, in this work we choose to detect the presence of Cu^{1+} (transit from Cu^{2+}), which is a direct result of the existence of oxygen vacancies. Electron energy loss spectroscopy (EELS) is a multifunctional spectroscopy for measuring atomic composition, chemical bonding, surface properties, conduction band electronic properties and especially the change of valence state.[16] Since such methods can readily distinguish Cu^{2+} and Cu^{1+} and it is more sensitive to low concentration of oxygen vacancies and less depend on sample crystalinity due to damage by electron irradiation,[17] the physical/chemical property changes that are

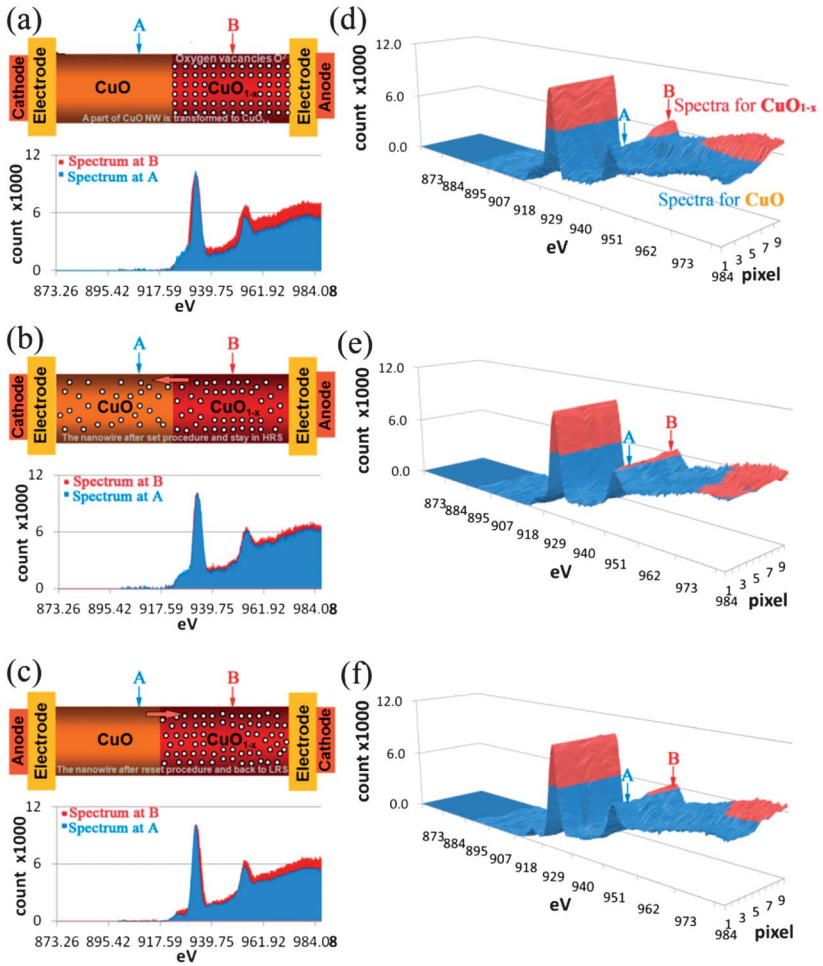

Fig. 4 The proof of the migration of oxygen vacancies. (a) The model of the nanowire after the forming process. After the forming of a part of the CuO NW to CuO_{1-x}, the oxygen cations are excessive in this segment due to the loss of oxygen atoms. The spectrum at B shows more oxygen vacancies than the spectrum at point A. (b) The model of the nanowire after the set procedure (from HRS to LRS). Set procedure: the anode is placed on the CuO_{1-x} and the cathode is in the CuO side. By sweeping the bias between two electrodes, the vacancies in CuO_{1-x} part are transported all through the nanowire, driven by the electric force. Meanwhile, the electrons pass through the conductive paths that are explored by the cations. Therefore, the conductivity is decreased. The gap between the spectrum at point A and point B is narrowed, which indicates the migration of oxygen vacancies from B to A. (c) The model of the nanowire after the reset procedure (from LRS to HRS). To switch from LRS to HRS (reset procedure), the electric force direction was switched according to the alternation of external poles, which in turn broke the conductive path along the nanowire and returns the resistance back to the original high status. The gap between the two spectra opened again, which indicates the reversal in migration of the oxygen vacancies from A to B. (d) The STEM-EEL spectra of the CuO NW after the forming process. The spectra topology represents the oxygen vacancy density difference along the nanowire. (e) The STEM-EEL spectra of the CuO NW after the set procedure. The spectra topology clearly indicates the migration of the oxygen vacancies from the rich area (B) to the poor area (A). (f) The corresponding STEM-EEL spectra for the CuO NW after the reset switching process. The reversal of O^{2-} migration is clearly indicated.

responsible for the memristive switching can be studied *in situ* using the EELS technique.

Cu $L_{2,3}$ edge spectra (Fig. 3(a)) at two distinctive areas on the nanowire with the pristine unirradiated portion (CuO) and the irradiated portion (CuO_{1-x}). The standard Cu^{2+} and Cu^{1+} spectra superimposed are inserted as a reference, showing the distinctive difference between the L_3/L_2 peak intensity ratio for Cu^{2+} and Cu^{1+}. The spectrum before the irradiation coincides with Cu^{2+} very well, proving its 100% CuO composition, while the spectrum after the irradiation lies in between that of Cu^{2+} and Cu^{1+}. Therefore, the irradiated part can be represented by CuO_{1-x} which is a mixture of Cu_2O and CuO. The creation of Cu^{1+} after the irradiation proves the loss of oxygen, *i.e.*, creation of oxygen vacancies. The amount of oxygen vacancies is qualitatively represented by the excessive L_2 peak intensity relative to that of Cu^{2+}. The Cu $L_{2,3}$ edge is at the unirradiated CuO area (point A) before and after the memristor setting process, *i.e.*, an applied voltage greater than V_{th}. It is clear that the spectrum after the switching voltage has a higher L_2 peak intensity than that before, indicating the presence of oxygen vacancies. Since there is no loss of overall oxygen atoms by applying a voltage, the oxygen vacancies can only have migrated from the CuO_{1-x} area.

Now a complete mechanism for CuO NW-based memristors can be illustrated schematically (Fig. 4). The initial forming process de-oxidizes CuO thus creates abundant oxygen vacancies, represented by small circles (Fig. 4(a)). However, these localized oxygen vacancies do not conduct through the nanowire, so the nanowire will stay at a high resistivity off state. The oxygen vacancies are forced to migrate under an external bias and eventually channel through the nanowire when the voltage reaches the threshold V_{th} (Fig. 4(b)). Then, the oxygen vacancies become the major dopants such that the nanowire switches to a low resistivity on state. Oxygen vacancies will remain as the dopants thus "remember" its low resistivity state. Only when a high reverse resetting threshold voltage is applied, the oxygen vacancies are forced to reverse their migration and eventually disconnect the conduction path (Fig. 4(c)). Then the nanowire device returns to its high resistivity off state. Again, with a bias lower than the setting voltage applied, it will remember its high resistivity state.

As we carried out the EELS measurement in a scanning transmission electron microscope (STEM), the EEL spectra along the nanowire can be continuously measured. A scanning oxygen EEL spectrum topology along the nanowire can be plotted, and the oxygen distributions *in situ* before and after the set process or reset process can be documented. Then, by comparing these spectrum topologies, the migration trend of the oxygen vacancies can be measured, which in turn provides solid evidence for the migration-based switching. The STEM-EELS technique was carried out across the nanowire from point A to point B (Fig. 4(a)). The continuous Cu $L_{2,3}$ edge EELS profile as plotted (Fig. 4(d)–(f)) correspond to each state in Fig. 4(a)–(c), respectively. Fig. 4(d) represents the spectra profile from point A to B at the initial state after forming, corresponding to Fig. 4(a). In order to give a clear visual effect, we deliberately set the color scheme so that the red color is directly correlated to the excessive L_2 peak intensity above that of Cu^{2+}. Therefore, the fact that there is no red signal at point A area further indicates that there are no oxygen vacancies. The excessive intensity of L_2 at point B is represented as a red color, representing the oxygen vacancies qualitatively. Moreover, the spectra at points A and B were also plotted (Fig. 4(a)). It is noted that there is a large gap between these two spectra, indicating the oxygen vacancies density difference at these two points. However, the gap between these two spectra was narrowed after the set switching process

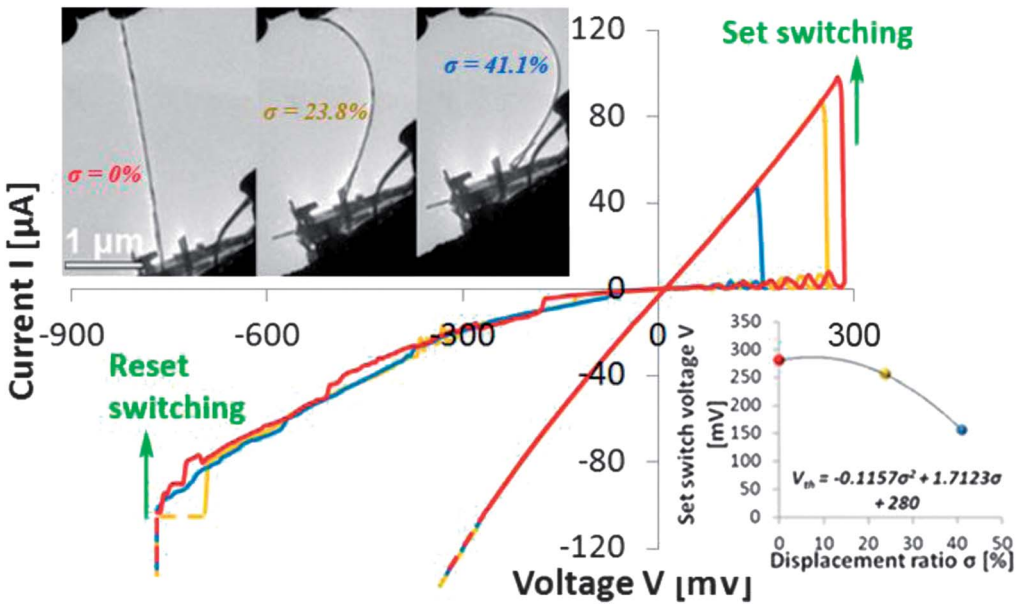

Fig. 5 The application of CuO NW-based memristor as a displacement transducer. The switching threshold voltage V_{th} was decreased according to the increasing of the deformation ratio σ. The displacement of the attached probe is measured by the deformation of the bending wire. The relations between the switching threshold voltage V_{th} and the displacement ratio σ can be read out as: $V_{th} = -0.1157\sigma^2 + 1.7123\sigma + 280$.

(Fig. 4(b)), which implies that the oxygen vacancies have changed at these two points. Furthermore, it is noted that there is clearly a red signal at L_2 peak for point A area from the spectral profile (Fig. 4(e)), accompanied by a slightly reduced red signal at area B. This is a direct evidence of the migration of the oxygen vacancies from B to A. After the reset switching process, the spectra profile (Fig. 4(f)) shows the disappearance of the red signal at L_2 peak in area A and the gap between the spectra in A and B (Fig. 4(b)) was opened again, indicating the reversal of oxygen vacancy migration.

Memsensor

In addition to the commonly anticipated NVRAM applications using memristors, we explore the possibility for "memsensors" based on a nanowire memristor that has a "memory" of other physical quantities, such as mechanical deformation/force.

The characteristic *I–V* curves at various deformations applied to the CuO NW are demonstrated (Fig. 5). By measuring the variation of set switching bias during the stressing, the nanowire displacement can be achieved, forming a displacement transducer. The switching threshold voltage V_{th} was decreased from 280 mV to 155 mV when the nanowire was deformed. The nanowire is bending as the attached probe is moved back and forth. The straight distance between the two terminals of the nanowire is reduced due to the compression. We define the deformation ratio as σ, as the reduction of the terminal distance relative to the original one. The displacement of the attached probe is measured by the deformation of the bending wire accordingly. Thus, the relations between the deformation ratio and the V_{th} can be expressed as: $V_{th} = -0.1157\sigma^2 + 1.7123\sigma + 280$.

This result strongly implies that we may have achieved a new device that we have defined as a "memsensor". For instance, without an external stress, when the voltage was kept at a constant intermediate value, *e.g.* 200 mV, the nanowire should keep its resistance since it is below the threshold voltage. By applying an external stress, it is possible to lower the memristor switching threshold voltage V_{th} below 200 mV, thus the memristor will have a transition from high resistance state to the low resistance state. Also, it will remain at the low resistance state even if the stress is withdrawn. In other words, this memristor will have memory of external stress instead of external voltage. It demonstrated the principle of a memsensor can be achieved by combining memristor properties with other sensory properties. While the detailed mechanism of CuO under stress is not fully understood yet, one of the interpretations is that the CuO NW may have piezoelectric properties which generate extra voltage under a stress.

Conclusions

In summary, we have developed a memristor nanodevice based on an individual CuO NW. The forming process depends on irradiation-beam-induced local de-oxidization of a segment of a CuO NW. The memristivity of this device is characterized by dynamic hysteretic current–voltage curves. By using the EELS technique to investigate the switching mechanism, we have not only confirmed the creation of oxygen vacancies in CuO NWs by the forming process, but also *in situ* quantified the migration of the oxygen vacancies, which is responsible for the memristive switching in our memristor device. The nanowire-based memristor has the potential to be combined with other sensing elements to form new types of memsensor devices. One such memsensor has been demonstrated with a combination with a mechanical displacement sensor. Therefore, nanowire-based memristors show great potential for designing all kinds of low-power high-throughput memory units and other functional nanodevices.

Acknowledgements

This work is partly supported by NSF (IIS-1054585).

References

1 D. B. Strukov, G. S. Snider, D. R. Stewart and R. S. Williams, *Nature*, 2008, **453**, 80–83.
2 D. S. Jeong, H. Schroeder, U. Breuer and R. Waser, *J. Appl. Phys.*, 2008, **104**, 123716.
3 B. J. Choi, D. S. Jeong, S. K. Kim, C. Rohde, S. Choi, J. H. Oh, H. J. Kim, C. S. Hwang, K. Szot, R. Waser, B. Reichenberg and S. Tiedke, *J. Appl. Phys.*, 2005, **98**, 033715.
4 J. J. Yang, M. D. Pickett, X. M. Li, D. A. A. Ohlberg, D. R. Stewart and R. S. Williams, *Nat. Nanotechnol.*, 2008, **3**, 429–433.
5 D.-H. Kwon, K. M. Kim, J. H. Jang, J. M. Jeon, M. H. Lee, G. H. Kim, X.-S. Li, G.-S. Park, B. Lee, S. Han, M. Kim and C. S. Hwang, *Nat. Nanotechnol.*, 2010, **5**, 148–153.
6 R. Waser and M. Aono, *Nat. Mater.*, 2007, **6**, 833–840.
7 W. Z. Wu and Z. L. Wang, *Nano Lett.*, 2011, **11**, 2779–2785.
8 Q. Liu, J. Sun, H. B. Lv, S. B. Long, K. B. Yin, N. Wan, Y. T. Li, L. T. Sun and M. Liu, *Adv. Mater.*, 2012, **24**, 1844–1849.
9 Y. C. Yang, P. Gao, S. Gaba, T. Chang, X. Q. Pan and W. Lu, *Nat. Commun.*, 2012, **3**, 732.
10 F. Mumm and P. Sikorski, *Nanotechnology*, 2011, **22**, 105605.
11 X. C. Jiang, T. Herricks and Y. N. Xia, *Nano Lett.*, 2002, **2**, 1333–1338.
12 D. S. Jeong, H. Schroeder and R. Waser, *Electrochem. Solid-State Lett.*, 2007, **10**, 51–53.
13 L. A. Bursill and A. C. McLaren, *Phys. Status Solidi B*, 1966, **13**, 331–343.
14 Z. L. Liao, P. Gao, X. D. Bai, D. M. Chen and J. D. Zhang, *J. Appl. Phys.*, 2012, **111**, 114506.
15 Y. M. Kim, J. He, M. D. Biegalski, H. Ambaye, V. Lauter, H. M. Christen, S. T. Pantelides, S. J. Pennycook, S. V. Kalinin and A. Y. Borisevich, *Nat. Mater.*, 2012, **11**, 888–894.
16 R. F. Egerton, *Electron energy-loss spectroscopy in the electron microscope*, Springer, New York, 3rd edn, 2011.
17 R. D. Leapman, L. A. Grunes and P. L. Fejes, *Phys. Rev. B: Condens. Matter Mater. Phys.*, 1982, **26**, 614–635.